NASA/TM—2015-218887

Effect of Notches on Creep-Fatigue Behavior of a P/M Nickel-Based Superalloy

Jack Telesman, Timothy P. Gabb, Louis J. Ghosn, and John Gayda, Jr.
Glenn Research Center, Cleveland, Ohio

November 2015

NASA STI Program . . . in Profile

Since its founding, NASA has been dedicated to the advancement of aeronautics and space science. The NASA Scientific and Technical Information (STI) Program plays a key part in helping NASA maintain this important role.

The NASA STI Program operates under the auspices of the Agency Chief Information Officer. It collects, organizes, provides for archiving, and disseminates NASA's STI. The NASA STI Program provides access to the NASA Technical Report Server—Registered (NTRS Reg) and NASA Technical Report Server—Public (NTRS) thus providing one of the largest collections of aeronautical and space science STI in the world. Results are published in both non-NASA channels and by NASA in the NASA STI Report Series, which includes the following report types:

- TECHNICAL PUBLICATION. Reports of completed research or a major significant phase of research that present the results of NASA programs and include extensive data or theoretical analysis. Includes compilations of significant scientific and technical data and information deemed to be of continuing reference value. NASA counter-part of peer-reviewed formal professional papers, but has less stringent limitations on manuscript length and extent of graphic presentations.

- TECHNICAL MEMORANDUM. Scientific and technical findings that are preliminary or of specialized interest, e.g., "quick-release" reports, working papers, and bibliographies that contain minimal annotation. Does not contain extensive analysis.

- CONTRACTOR REPORT. Scientific and technical findings by NASA-sponsored contractors and grantees.

- CONFERENCE PUBLICATION. Collected papers from scientific and technical conferences, symposia, seminars, or other meetings sponsored or co-sponsored by NASA.

- SPECIAL PUBLICATION. Scientific, technical, or historical information from NASA programs, projects, and missions, often concerned with subjects having substantial public interest.

- TECHNICAL TRANSLATION. English-language translations of foreign scientific and technical material pertinent to NASA's mission.

For more information about the NASA STI program, see the following:

- Access the NASA STI program home page at http://www.sti.nasa.gov

- E-mail your question to help@sti.nasa.gov

- Fax your question to the NASA STI Information Desk at 757-864-6500

- Telephone the NASA STI Information Desk at 757-864-9658

- Write to:
  NASA STI Program
  Mail Stop 148
  NASA Langley Research Center
  Hampton, VA 23681-2199

NASA/TM—2015-218887

Effect of Notches on Creep-Fatigue Behavior of a P/M Nickel-Based Superalloy

Jack Telesman, Timothy P. Gabb, Louis J. Ghosn, and John Gayda, Jr.
Glenn Research Center, Cleveland, Ohio

National Aeronautics and
Space Administration

Glenn Research Center
Cleveland, Ohio 44135

November 2015

Acknowledgments

The authors wish to acknowledge the work of Andrew Ring in conducting mechanical testing and Joy Buehler in performing the metallography. The work was funded by NASA's Aviation Safety program.

Level of Review: This material has been technically reviewed by technical management.

Available from

NASA STI Program
Mail Stop 148
NASA Langley Research Center
Hampton, VA 23681-2199

National Technical Information Service
5285 Port Royal Road
Springfield, VA 22161
703-605-6000

This report is available in electronic form at http://www.sti.nasa.gov/ and http://ntrs.nasa.gov/

Effect of Notches on Creep-Fatigue Behavior of a P/M Nickel-Based Superalloy

Jack Telesman, Timothy P. Gabb, Louis J. Ghosn, and John Gayda, Jr.*
National Aeronautics and Space Administration
Glenn Research Center
Cleveland, Ohio 44135

Abstract

A study was performed to determine and model the effect of high temperature dwells on notched low cycle fatigue (NLCF) and notch stress rupture behavior of a fine grain LSHR powder metallurgy (P/M) nickel-based superalloy. It was shown that a 90 sec dwell applied at the minimum stress ("min dwell") was considerably more detrimental to the NLCF lives than similar dwell applied at the maximum stress ("max dwell"). The short min dwell NLCF lives were shown to be caused by growth of small oxide blisters which caused preferential cracking when coupled with high concentrated notch root stresses. The cyclic max dwell notch tests failed mostly by a creep accumulation, not by fatigue, with the crack origin shifting internally to a substantial distance away from the notch root. The classical von Mises plastic flow model was unable to match the experimental results while the hydrostatic stress profile generated using the Drucker-Prager plasticity flow model was consistent with the experimental findings. The max dwell NLCF and notch stress rupture tests exhibited substantial creep notch strengthening. The triaxial Bridgman effective stress parameter was able to account for the notch strengthening by collapsing the notched and uniform gage geometry test data into a singular grouping.

Introduction

A new generation of powder metallurgy (P/M) disk superalloys has been designed for higher engine operating temperatures by improvement of their strength and creep resistance. This increase in the engine operating temperatures has resulted in additional emphasis being placed on high temperature environmental resistance and dwell behavior of these alloys to determine their long term high temperature durability. The increased strength and creep resistance of these alloys may also increase their notch sensitivity to fatigue loading and thus have a profound effect on the notched low cycle fatigue life. NLCF is a key mechanical property of the highly stressed gas turbine rotating components since it simulates behavior at notches and bolt holes which are the regions from where the majority of failures of rotating components tend to originate (Ref. 1).

With the increase in the disk operating temperatures, sustained dwells applied at the maximum stress have been shown to significantly degrade both smooth and notched LCF fatigue life (Refs. 2 to 4). More surprising has been a finding by Bache et al. (Ref. 5) that an imposition of a 90 sec dwell at the minimum stress produced an even greater reduction in NLCF life. This was also confirmed in our study of the ME3 disk alloy (Ref. 6). The differences in the notch fatigue life response to max dwell and min dwells are thought to be influenced by both notch stress relaxation and environmental degradation (Refs. 5 and 6), but more work remains to be performed to further understand the mechanisms by which these interactions occur.

The presence of notches adds another level of complexity to the already complex world of environment-load history interactions. The resulting multiaxial stress state at the notch root, combined with visco-plastic high temperature material response, can produce significant redistributions of stresses and strains in the notch region which in turn affect the life and the overall durability of the disk alloys. The role that axial stress, hydrostatic stress and the effective stress play in determining the durability needs to be sorted out. Due to these complexities, currently available life prediction models are not able to

* Retired.

accurately predict dwell notched low cycle fatigue life. Formulation of more accurate life prediction models requires an improved understanding of the damage mechanisms responsible for material degradation and accumulation of fatigue damage. The key to gaining this understanding is the identification of the active material damage mechanisms for a given set of test conditions and their relationship to the redistribution of the notch root stresses and strains which takes place during the prolonged dwells.

The approach of the current study was to isolate as much as possible the major variables which affect the dwell NLCF behavior so that their individual mechanistic contributions to material durability could be studied, quantified and modeled. The work was performed by testing the NASA developed LSHR P/M disk alloy. A variety of test types were conducted to characterize the material behavior. Cyclic, cyclic-dwells, stress-rupture and creep testing was performed using both notch and uniform section specimen geometries to characterize material response under varied loading conditions. Baseline cyclic tests were performed as well as notch dwell fatigue tests with 90 sec holds at either maximum or minimum stress. The application of 90 sec dwells at the min stress was utilized so that the role of the environment can be studied without the complication of visco-plastic stress redistribution. Notch and smooth stress-rupture testing was used to quantify the creep contribution to the damage process. While most of the testing was performed in lab air, selected specimens were tested in vacuum to isolate and quantify the environmental contribution to the damage evolution.

This paper will compare the pronounced effect that both environmental damage and the visco-plastic stress redistribution have on the lives of LSHR specimens. The aim of the study is to identify the key parameters which account for these differences in behavior and to present a methodology which can explain and predict these results.

Materials and Procedure

The LSHR P/M alloy with a composition consisting in weight percent of 20.7 Co, 4.3 W, 3.5 Al, 3.5 Ti, 2.7 Mo, 1.6 Ta, 1.5 Nb, 0.05 Zr, 0.03C, 0.03 B with balance Ni was used in the study. Small pancake forgings approximately 15 cm in diameter and 3.7 cm thick of this composition were heat treated as follows to produce a fine grain subsolvus microstructure: solution at 1135 °C, fan cooled and aged at 855 °C/4 hr + 775 °C/8 hr. The heat treatment produced a fine grain microstructure approximately 5 to 10 μm in diameter (ASTM 11-12). Specimens were machined from heat treated forgings. Approximate cooling rate from the solutioning temperature was designated for the location of each blank removed from the pancake forgings.

Testing consisted of cyclic notch fatigue, cyclic notch dwell fatigue, creep notch rupture, combo-bar creep and uniform gage creep tests. The details of all the test conditions are shown for the cyclic and cyclic dwell NLCF tests in Table I and for the creep and stress rupture tests in Table II. Specimen geometry of the notched bars are shown in Figures 1 and 2. All the notched bars had an elastic stress concentration factor (K_t) of 2.0. Combo-bar geometry, shown in Figure 3, consists of a uniform gage section and a notched region with the notch diameter being equal to that of the smooth section. All testing was performed at 704 °C. Three different waveforms were utilized: sinusoidal with frequencies of 10 Hz and 0.333 Hz, max dwell (1.5-90-1.5) seconds and min dwell (1.5-1.5-90) seconds with dwell cycles shown in Figure 4. As shown in Tables I and II, in addition to lab air, selected tests were performed in vacuum. The testing was conducted at various net section stresses ranging from 483 to 896 MPa with the majority of the tests being conducted at 793 MPa to determine the data repeatability.

Stress relaxation testing was conducted at 704 °C to obtain a constitutive creep relationship for the alloy for use in the visco-plastic modeling. Stress relaxation was measured after a 1 percent total strain was achieved in a standard tensile test. The specimen was then held at 1 percent strain for 100 hr while the change in stress was monitored by an automated data acquisition system. Visco-plastic axi-symmetric finite element analysis was performed on the notch specimen geometry to determine the redistribution of notch root stresses. Both von Mises and Drucker-Prager plasticity flow models embedded in the ABAQUS finite element code (Ref. 7) were used for the analysis.

Results and Discussion

Nonunified Visco-Plastic FEM Analysis of Notch Root Stresses

The evolution of the notch root stresses was modeled using finite element modeling (FEM) as a function of the number of applied cycles for both max dwell and min dwell loading profiles. The notched specimen geometry was modeled with two-dimensional axi-symmetric nonlinear elements and the material modeled using a nonunified viscoplastic analysis wherein the strain is decomposed into separate elastic, plastic, creep, and thermal components.

The inelastic strain was computed using both classical von Mises and Drucker-Prager plasticity flow models within ABAQUS, the required material parameters being obtained from the tensile and stress relaxation data. The stress relaxation material response was correlated using the following creep law:

$$\dot{\varepsilon} = A\sigma^n t^m + B\sigma^p \tag{1}$$

where $\dot{\varepsilon}$ is the strain rate, σ is the equivalent creep stress defined as either von Mises stress for the von Mises flow model or the effective creep stress for the Drucker-Prager model function of the von Mises stress and the hydrostatic stress, t is time and A, B, n, m and p are fitting constants. The creep coefficients which fit this equation were determined and are shown in Figure 5 together with the comparison to the experimentally obtained stress relaxation results. The notch stress distribution profiles for various types of stress components were calculated for both max and min dwell loading histories. The results of the FEM analysis will be discussed later to help explain experimental results for each type of the loading history investigated.

Notch Cyclic and Dwell Fatigue Behavior

Comparison of notch low cycle fatigue results for the three waveforms used in the study is shown in Figure 6 and Table I. All the tests shown in the figure were performed in lab air with a maximum applied net section stress of 793 MPa. As shown, the fatigue lives were highly dependent on the applied waveform. The high frequency cyclic notch fatigue tests exhibited fatigue lives in the order of 250,000 cycles. Reduction of frequency from 10 to 0.333 Hz resulted in notch LCF lives of approximately 150,000 cycles. Imposition of a 90 sec hold at the maximum stress had a very significant effect on NLCF with the specimens failing in the range of 15,000 to 35,000 cycles. Further significant reduction in fatigue lives occurred when the 90 sec dwell was applied at the minimum stress. As shown in Figure 6, the dwell notch fatigue lives for the min dwells were approximately an order of magnitude lower in comparison to the max dwell tests. While these results are somewhat counter-intuitive, they are in agreement with the trends observed by Bache et al. for RR1000 (Ref. 5) as well as in our study of the ME3 alloy (Ref. 6).

Fractographic examination of specimens tested utilizing the three waveforms revealed that the failure mode differed substantially for each type of test as shown in Figure 7. For the high frequency cyclic baseline tests only a single initiation site located near the notch surface was observed (Fig. 7(a)) from which the crack propagated internally until failure occurred. Higher magnification images of the initiation site (Fig. 8) revealed that the crack initiated from a near surface inclusion which was present in this high stress concentration region. This is a well-known failure mode in P/M disk superalloys and is not significantly influenced by the environment since the initiations often occur in the subsurface region.

In contrast to the single fatigue crack initiation site for specimens tested using high frequency waveform, the 90 sec min dwell tests produced multiple fatigue crack surface initiation sites around the notch root perimeter as shown Figure 7(b). These multiple cracks coalesced and caused the specimen to fail. A more detailed discussion of this environmentally influenced failure mode will be presented in the next section. The 90 sec max dwell tests failure mode was radically different from the two already described. As shown in Figure 7(c), the primary initiation site was internal at a substantial distance away from the notch root. In addition to the primary internal initiation site, a single small secondary surface

initiation region was also present as also marked in Figure 7(c). The shift in the location of the primary failure away from the notch root points to the crucial role that visco-plastic stress redistribution can play in controlling the damage evolution process. This topic will be discussed extensively in this paper.

Cyclic Minimum Dwell Notch Fatigue

As was shown in Figure 7(b), the min dwell notch LCF testing resulted in multiple surface initiations which produced short fatigue lives in the order of 2000 to 5000 cycles when tested in air at maximum net section stress of 793 MPa. A more detailed fractographic initiation examination revealed the presence of a multitude of cracks at the notch root surface. As shown in Figure 9, these cracks typically initiated at oxide blisters which formed at the notch root surfaces during testing. The cause of the formation of these localized oxide blisters has not been established in this study but in our previous study of ME3 (Ref. 6) similar blisters originated either from the oxidation of MC-type carbides (M = Ti, Nb, W, Ta) or were due to local heterogeneities in the microstructure. Recently, O'Hanlon et al. (Ref. 8) also documented these type of features causing early crack initiation during min dwell tests. As shown in Figure 9, these oxidized areas are only few microns in width, yet due to the high stresses at the notch root these brittle particles fracture and initiate cracks. In essence, the growth of the brittle oxidized particles can be considered to be analogous to the presence of ceramic inclusions which are also known to initiate cracks when exposed to high enough cyclic stresses. The difference being that the oxidized blisters form and grow during the test itself while ceramic inclusions are present from the outset.

To confirm that the environment is indeed the culprit in reducing the notch dwell fatigue lives for min dwell testing, a test was conducted in a vacuum test chamber under the same loading conditions. As shown in Figure 10, the min dwell notch fatigue life of the specimen was approximately 39,000 cycles and thus an order of magnitude longer than the tests performed in air. It should be noted that the life of the vacuum specimen would likely have been even longer, since an improper bake out of a new heating element installed at approximately 28,600 cycles coated the specimen with a thin layer of a brittle ceramic phase. An array of cracks formed in this layer upon the restart of the test, with these cracks growing into the substrate and shortening the specimen's life. The specimen notch surface which was examined in the SEM at 28,600 cycles prior to the installation of the new heating element shows the notch in almost pristine condition with no apparent cracks (Fig. 11(a)). As shown, after 28,600 cycles no oxide blisters or cracks were present on the notch root surface. This is in stark contrast to the min dwell notch specimens tested in air where a multitude of cracks were present after only few thousand cycles. Thus the relationship between oxidation damage and min dwell notch fatigue life is quite evident. The same vacuum specimen examined after failure at approximately 39,000 cycles shows an array of cracks originating from the inadvertently deposited brittle coating (Fig. 11(b)). The vacuum test has not as yet been repeated due to the unavailability of the test rig.

In addition to the presence of brittle oxide blisters, surface stresses high enough to fracture these brittle particles are required for crack initiation to occur. The evolution of notch root stresses was modeled for the min dwell tests through FEM analysis. Figure 12, shows the stress distribution profiles for the first forty min dwell cycles as a function of the distance from the notch root in terms of axial, von Mises and hydrostatic stresses. While there is a small change in stresses after the first cycle, all the subsequent cycle stress distributions lie directly on top of each other. The figure shows that for all three stress types, stresses are highest in the near notch root region and drop off significantly as a function of distance away from the notch. The calculated notch root axial maximum stresses are approximately 1300 MPa while the von Mises stresses approach 1100 MPa and thus both are still considerably higher than the 793 MPa applied net section stress. This is not surprising since the 90 sec min dwells occur at stresses where compressive creep is minimal and has no significant effect on the visco-plastic evolution of maximum notch root stresses.

To better understand the inter-relationship between oxidation damage and the surface stresses, a 90 sec min dwell test was performed in air using a uniform gage specimen geometry. This test was performed at the same 793 MPa net section stress as was done for the notch specimens. After no failure

occurred during the first 50,000 cycles, the test was stopped and the specimen surface was examined in the SEM. As shown in Figure 13, while the specimen surface is covered with oxide particles, no surface cracking was detected on the oxide covered surface. Thus, for the uniform gage specimen, the 793 MPa applied max stress was too low to crack the thin, brittle oxide layer. Without the onset of early cracking from oxide blisters, the min dwell fatigue life is considerably longer for the uniform gage specimens than for notched min dwell tests performed at the same net section stress.

Cyclic Maximum Dwell Notch Fatigue and Notch Rupture Testing

As shown earlier, the life of the cyclic max dwell notch tests performed at the 793 MPa net section stress was considerably higher than for the min dwell tests performed at the same maximum stress (Fig. 6). It was also shown (Fig. 7(c)) that in contrast to the cyclic and the min dwell cyclic tests tested conducted at the same stress, the primary crack initiation shifted internally at a considerable distance away from the notch root. Fractography of some the other cyclic max dwell notch tests showed similar behavior (Fig. 14(a)). The measured distances from the notch root to the internal initiation locations for the various specimens is shown in Table III. As shown, while there is a considerable scatter, most of the internal initiations occurred at distances ranging from 1 to 2.5 mm away from the notch root. A companion test performed in vacuum not only revealed a similar internal initiation mechanism (Fig. 14(b)), but also had a fatigue life similar to the other cyclic max dwell notch specimens tested in air (Fig. 14(c)). The comparable fatigue life for both air and vacuum tests is due to the environment not being a major factor in influencing the life of the specimen due to its internal initiation.

Further fractographic examination of the internal initiation locations revealed extensive plastic deformation near the crack origins. These features were consistent with failure by a creep deformation process (Fig. 15) and not by a fatigue process. For all the internal initiations examined, no fractographic evidence of fatigue failure mechanisms were observed near the internal initiation regions. It should be noted that while most of the cyclic max dwell notch test specimens tested at 793 MPa net section stress exhibited a primary internal initiation, many also exhibited a secondary near surface initiations which likely are a result of fatigue (Fig. 16).

If creep damage accumulation, and not fatigue, was the primary failure mechanism for these cyclic notch max dwell tests, then the notch creep rupture tests conducted at the same temperature and net section stress should also result in similar time to failure and exhibit the same failure mechanisms. The comparison of test results in terms of time to failure between the max dwell tests and notch rupture tests is shown in Figure 17. As shown, the time to failure is similar for both types of tests even though significant scatter is also present. Further evidence for the creep deformation being the dominant damage accumulation mechanism is obtained through the comparison of the fractographic and metallographic analyses of the two test types. As shown in Figure 18, the crack initiation location for the creep notch rupture tests is also internal and has very similar appearance to the cyclic notch max dwell tests (Figs. 7 and 14). A comparison of metallographic cross sections of the cyclic notch max dwell tests and the creep notch rupture tests obtained slightly below the fracture plane is shown in Figure 19. Both types of tests exhibited the classical creep damage accumulation through formation and coalescence of voids at grain boundaries thus confirming the dominant role that creep deformation played in these two test types. Our findings are in agreement with previous work performed by Pandey et al. (Ref. 9) on Inconel alloy X-750. In their work, they also found that crack initiations in notch creep rupture specimens occurred at a substantial distance away from the notch root.

One difference not discussed as yet between the fractography of the cyclic notch max dwell tests and creep notch rupture tests was the presence of the secondary notch root surface crack initiation regions. While these surface secondary initiation sites were present in most of the 793 MPa cyclic max dwell tests (Figs. 7 and 14), they were completely absent in the creep notch rupture tests (Fig. 18). Even though extensive visco-plastic stress redistribution occurs during max dwells, if the remaining notch root cyclic stress range is high enough, fatigue cracks can still initiate. Creep notch rupture tests do not exhibit these surface initiations since they are not exposed to cyclic loading. It is interesting to note that cyclic notch

max dwell tests which were performed at higher next section stress of 896 MPa exhibited only notch root surface initiations (Fig. 20). It is thought that at this higher applied net section stress, the notch root cyclic stress range was high enough to cause earlier fatigue crack initiation which dominated the failure process.

Creep and Combo Creep Test Results

The results of the uniform gage creep tests performed in air and vacuum are shown in Figure 21 and also in Table II. The testing was conducted at the maximum net section stresses ranging from 483 to 896 MPa. At the highest applied stress, the four tests performed in air failed between 25 to 35 hr, while the two tests performed in vacuum failed after 55 and 90 hr, respectively. This difference in creep life between air and vacuum tests disappeared at lower stresses as shown in Figure 21 with both air and vacuum uniform gage specimens exhibiting similar time to failure.

In addition to the smooth specimens, creep rupture tests were performed on six combo-bar specimens of the geometry shown in Figure 3. All the combo-bar tests were done at 793 MPa. All six combo-bar failures occurred strictly in the uniform gage region. The lives of the combo-bar specimens were very similar to the uniform gage creep specimens as shown in Figure 22. For comparison, the much longer notch creep rupture and cyclic dwell NLCF lives are also shown in this figure.

It is interesting to note the differences in the failure mechanisms of the uniform gage creep tests performed in air and in vacuum. As shown in Figure 23(a), the creep test conducted in air exhibited a multitude of surface cracks which initiated at the oxidized blisters formed during the test. These oxide cracks are perpendicular to the loading direction. Also as shown, the main crack initiation region in this specimen occurred on the specimen surface. The surface cracking from environmentally created brittle oxide regions is reminiscent of the oxide induced early crack initiation and surface failure of the cyclic min dwell tests discussed previously.

In contrast, the vacuum tested uniform gage creep specimen exhibited a markedly different appearance. As shown in Figure 23(b), on the machined surface of the specimen only shear plastic deformation bands are present resulting in cracks angular to the loading direction. The specimen surface appearance is that of a material which has experienced extensive plastic deformation. Examination of the fracture surface revealed that the crack initiation occurred internally in the mid-thickness region of the specimen (Fig. 23(b)). Thus the presence of a brittle, oxidized phases on the surface can significantly alter the damage accumulation process.

Modeling of the Visco-Plastic Notch Root Stress Redistribution

The shift in the failure initiation location away from the root of the notch towards interior regions of the specimens, as was experienced in both cyclic notch max dwell tests and creep notch rupture tests, must be fully understood so that accurate life prediction models can be developed. Stress redistribution due to the presence of the notch was modeled using a number of different approaches to determine the applicable methodology which can best predict the observed behavior. The resulting stress distribution profiles were compared to the observations in terms of the location of the maximum stress which is assumed to control the initiation process.

An axi-symmetric visco-plastic FEM analysis was performed using the constitutive creep model previously derived (Fig. 5). The creep analyses were performed using both the von Mises and Drucker-Prager inelastic flow models embedded in ABAQUS to determine their ability to predict material behavior. The von Mises flow model is most commonly used for ductile metals. One of its theoretical assumptions is that the yield strength is independent of hydrostatic stresses. The resulting yield surface of the von Mises flow model is a circular cylinder. The Drucker-Prager yield criterion is rarely used to model metal inelastic behavior, however for high hydrostatic stresses, the model may be preferable to von Mises (Ref. 10). It differs in that in the model formulation, the effective inelastic stress is a function of the hydrostatic stress as the deviatoric stress. In terms of the yield surface, Drucker-Prager yield function results in a conical yield surface.

The results of the visco-plastic analysis using the von Mises plasticity flow model are shown in Figure 24 in terms of the stress distribution profiles for the axial, von Mises and hydrostatic stresses. The figure shows these stress profiles at the beginning of the test as well as after 1000 hr at the sustained max dwell. As shown, a significant redistribution of all three stress types occurs after the 1000 hr dwell. After the dwell, the von Mises stresses are still considerably higher at the notch root than in the interior regions and thus they do not predict the observed behavior. Both the axial and hydrostatic stresses after 1000 hr of creep calculated using the von Mises flow model are still the highest near the notch root with the peak stress being approximately 0.4 mm below the surface. The measured location of failure initiation sites for the tested specimens is shown both in Table III and graphically superimposed onto Figure 24. As shown, the actual initiation locations are considerably deeper and do not correspond to either the axial or hydrostatic stress distributions shown in the figure. Thus none of the three creep redistributed stress profiles generated by the von Mises plastic flow model are in agreement with the observed behavior.

The results for the Drucker-Prager flow model are shown in Figure 25. Again the stress profile distributions are shown for both the initial as well as 1000 hr max dwell conditions. As shown, after the dwell, neither the redistributed axial or von Mises stresses are in good agreement with the experimental results. The peak von Mises stresses are still at the notch root while the redistributed axial stresses are highest in the vicinity of the notch and are considerably higher in that region than at the depths at which the majority of the specimens' crack initiations occurred.

The hydrostatic stress profile after the application of 1000 hr dwell, shown in Figure 25, is considerably different than the other profiles already described. As shown, the lowest hydrostatic stresses are at the notch and rise gradually as a function of the distance from the notch root. They peak approximately 1 mm away from the notch and remain fairly uniform and close to the peak level over the entire distance to the center of the specimen. Thus the triaxial hydrostatic stress profile is in the agreement with the experimental observations of the location of the failure initiation sites for the cyclic max dwell and notch stress rupture tests performed at max stress of 793 MPa.

As described earlier and shown in Table III and Figure 25, the initiation locations are spread out in a region away from the notch. The lack of one distinct location for the initiations to occur can be explained by a relatively flat distribution of the hydrostatic stresses which allows for initiations to occur at the weakest point in the material over the region subjected to the high stresses.

Bridgman Effective Stress Analysis

Hydrostatic stress is the mean of the sum of the three principal stresses and thus its ability to explain the creep dominated failures in the tested notched specimens emphasizes the importance of stress triaxiality under highly plastically deformed notch conditions. One of the earliest studies of the effect of stress multiaxiality on plastic deformation was performed by Bridgman (Ref. 11). Based on his analysis, he formulated an effective triaxial stress parameter, σ_e, to be as follows:

$$\sigma_e = \sigma_{\text{net}}\left[\left(1+\frac{2R}{a}\right)\ln\left(1+\frac{a}{2R}\right)\right]^{-1} \tag{2}$$

where σ_{net} is the net section stress, a is the distance from the center of the specimen to the notch root and R as originally defined was the radius of curvature of the neck down profile for a smooth specimen but being extended here to be the notch root radius.

The test data generated in the program for the notch and smooth specimen geometries was used to evaluate the ability of the Bridgman effective stress to correlate the cyclic max dwell and creep rupture behavior. For uniform gage specimens, the effective stress is equal to the net section stress while for the notch geometry used in the study the effective stresses were calculated per Equation (2). Both the notched and smooth test data is first plotted in terms of the applied net section stress and shown in Figure 26. As shown, the data can be grouped separately with the notched specimens exhibiting

considerably longer lives to failure in terms of the net section stresses than the uniform gage specimens. However when the same data set is plotted in terms of the Bridgman effective stress (Fig. 27), most of the data converges into a singular grouping. It should be noted that much of the scatter still present in the Bridgman effective stress plot shown in Figure 27 is due to the inherent variations in lives of specimens tested under "identical" conditions. No mechanistically derived parameter can account for that type of scatter. Thus, this methodology, which was developed many years ago, is still very useful in modeling notch-induced plastic deformation.

Finally, it should be noted that in our test program both "notch strengthening" and "notch weakening" was induced in the same material. As shown in Figure 26, substantial amount of notch strengthening occurred for the cyclic max dwell and creep notch rupture specimens. The notch strengthening was created by the extensive notch stress redistribution which occurred due to the creep strain accumulation at the notch root. In contrast, the cyclic min dwell testing produced a notch weakening effect. In that case, the notch region was embrittled by oxidation of the surface which took place during the dwells. Since the min dwell notch stress redistribution is rather limited, high concentrated notch stresses remained and caused early crack initiation in the oxidized notch region which led to much shorter fatigue lives. For the uniform gage specimens tested under the same cyclic min dwell conditions, the surface is also embrittled through oxidation, however, the applied net section stress was too low to cause initiation on the environmentally embrittled surfaces resulting in much longer fatigue life.

Summary

A study was performed to determine and model the effect of high temperature dwells on notched low cycle fatigue and notch stress rupture behavior of a fine grain LSHR disk alloy. The dwell cycles consisted of either 90 sec hold at the maximum stress or the minimum stress. While both dwell cycles significantly reduced the lives of the notched specimens in comparison to the no-dwell baseline NLCF, the min dwell tests resulted in the largest reduction in the notched low cycle fatigue lives. The severe reduction in the lives of the notched min dwell specimens was shown to be the result of formation of small surface oxide blisters during the dwells which cracked due to the high sustained concentrated notch root stresses. The FEM analysis of the min dwell NLCF tests showed that the notch root stresses remained high during the test duration causing multiple surface crack initiations from the oxidized and embrittled particles.

In contrast, the controlling failure initiation for the cyclic notch max dwell and notch rupture tests at comparable applied stresses typically occurred internally at a substantial distance away from the notch root. It was shown that the controlling damage accumulation mechanism for max dwell cyclic tests was creep and not fatigue. Stress redistribution due to the presence of the notch was modeled using a number of different approaches to determine the applicable methodology which can best predict the observed behavior. Both von Mises and Drucker-Prager flow models were examined and the axial, von Mises and hydrostatic stress profiles were generated for both flow models. None of the stress profiles generated using von Mises flow model was consistent with the experimental observations. Only the hydrostatic stress profile generated through the use of the Drucker-Prager flow model was consistent with the experimental results pointing to the controlling effect of stress triaxiality on the creep notch stress redistribution.

A Bridgman net section effective stress formulation which takes into account the triaxiality of state of stress along the notch plane was used to correlate the notched cyclic max dwell, notch stress rupture and uniform gage creep tests. While the data sets showed a pronounced notch strengthening effect when correlated using the net section stress parameter, the Bridgman effective stress parameter was able to more reasonably collapse the data into a singular grouping.

References

1. Schafrik R, Sprague R., “Superalloy Technology – A Perspective on Critical Innovations for Turbine Engines,” Key Engineering Materials, v. 380, 2008.
2. Gabb T.P., Gayda J., Telesman J., Ghosn L., Garg A.; Factors Influencing Dwell Fatigue Cracking in Notches of Powder Metallurgy Nickel Disk Alloy; Int. J. of Fatigue 48, 2013, 55–67.
3. Goswain T., Hanninen H., “Dwell Effects on High Temperature Fatigue Behavior – Part I,” Matl and Design vol. 22, 2001.
4. Greving D., Kantzos P., Neumann J., Rice D., Kington H.; “Dwell Notch Low-Cycle Fatigue Performance of Powder Metallurgy Alloy 10,” 12th Int. Symposium on Superalloys, Superalloys 2012.
5. Bache M.R., Jones J.P., Drew G., Hardy M., Fox N., “Environment and Time Dependent Effects on the Fatigue Response of an Advanced Nickel Based Superalloy,” Int. J. of Fatigue 31, 2009, 1719–1723.
6. Telesman J., Gabb T., Ghosn L., Yamada Y., Jayaraman N., “Dwell Notch Low Cycle Fatigue Behavior of A Powder Metallurgy Nickel Disk Alloy,” 12th Int. Symposium on Superalloys, Superalloys 2012.
7. ABAQUS Version 6.13-1, Dassault Systèmes Simulia Corp., Providence, RI, © Dassault Systèmes, 2013.
8. O’Hanlon J., Hardy M., Child D., Foss B., Withers P., Bache M.; “The effect of Minimum Dwell Cycles on the Environment and Fatigue Response of RR1000,” MATEC Web of Conferences 14, 04003, 2014.
9. Pandey M., Mukherjee A., “Effect of Triaxial Stress-State on Creep Fracture in Inconel Alloy X-750,” J. of Matl Science, vol. 20, 1985, 1201–1206.
10. Wilson C.; “A Critical Reexamination of Classical Metal Plasticity,” – J. of Applied Mechanics, vol. 69, Jan 2002.
11. Bridgman P.; Studies in Large Plastic Flow and Fracture with Special Emphasis on the Effects of Hydrostatic Pressure, McGraw-Hill, NY, 1952.

TABLE I.—DWELL AND CYCLIC NOTCH LCF TEST RESULTS

Specimen ID	Test type	Cooling rate from solutioning to 871 °C, °C/min	Test temp., °C	Max stress, MPa	Min stress, MPa	Hold time-seconds	Max/Min dwell; cyclic	Frequency, Hz	Cycles to failure	Time to failure, hr	Failure location
E2-N1	DNLCF-Kt=2 Air	64	704	793	40	90	Max	N/A	37361	955	Internal
E2-N2	DNLCF-Kt=2 Air	73	704	793	40	90	Max	N/A	38280	978	Internal
E2-N3	DNLCF-Kt=2 Air	73	704	793	40	90	Max	N/A	24452	625	Internal
E2-N4	DNLCF-Kt=2 Air	73	704	793	40	90	Max	N/A	42361	1083	Internal
E2-N5	DNLCF-Kt=2 Air	73	704	793	40	90	Max	N/A	14991	383	N. Surface
E2-N6	DNLCF-Kt=2 Air	73	704	793	40	90	Max	N/A	23897	611	Internal
C-N8	DNLCF-Kt=2 Air	71	704	793	40	90	Max	N/A	14248	364	N. Surface
C-N10	DNLCF-Kt=2 Air	71	704	827	41	90	Max	N/A	13443	344	N. Surface
C-N11	DNLCF-Kt=2 Air	71	704	793	40	90	Max	N/A	32104	820	Internal
C-N13	DNLCF-Kt=2 Air	68	704	793	40	90	Max	N/A	30541	780	Internal
C-N15	DNLCF-Kt=2 Air	68	704	896	45	90	Max	N/A	2123	54	N. Surface
C-N18	DNLCF-Kt=2 Air	76	704	827	41	90	Max	N/A	18793	480	Internal
9D-L1	DNLCF-Kt=2 Air	67	704	896	45	90	Max	N/A	5541	146	Surface
0A-L5	DNLCF-Kt=2 Air	71	704	793	40	90	Max	N/A	26128	675	Intern/surf
9D-L3	DNLCF-Kt=2 Air	71	704	690	34	90	Max	N/A	66249	1711	Internal
9C-L5	DNLCF-Kt=2 Air	71	704	690	34	90	Max	N/A	55396	1431	Internal
9D-L5	DNLCF-Kt=2; Vacuum	71	704	793	34	90	Max	N/A	44709	1180	Intern/surf
9D-L2	DNLCF-Kt=2; Vacuum	71	704	896	45	90	Max	N/A	14156	374	Surface
C-N9	DNLCF-Kt=2 Air	71	704	793	40	90	Min	N/A	3500	89	Surface
C-N17	DNLCF-Kt=2 Air	76	704	793	40	90	Min	N/A	4778	122	Surface
0F-L4	DNLCF-Kt=2 Air	71	704	793	40	90	Min	N/A	2200	58	Surface
0A-L2	DNLCF-Kt=2 Vacuum	71	704	793	40	90	Min	N/A	39106	1032	Surface
C-N1	NLCF Kt=2 Air	79	704	793	40	N/A	Cyclic	10	245105	7	N. Surface
C-N5	NLCF Kt=2 Air	66	704	793	40	N/A	Cyclic	10	297795	8	N. Surface
0A-L4	NLCF Kt=2 Air	71	704	793	40	N/A	Cyclic	0.333	173659	145	N. Surface
0A-L1	NLCF Kt=2 Air	67	704	793	40	N/A	Cyclic	0.333	153546	128	N. Surface

TABLE II.—UNIFORM GAGE CREEP, COMBO-BAR AND NOTCH RUPTURE TEST RESULTS

Spec ID	Test type	Cooling rate from Solutioning to 871 °C (°C/min)	Test temp, °C	Stress, MPa	Rupture life, hr
E2-T1	Creep -Air	70	704	896	35.4
E2-C1	Creep -Air	68	704	690	261.9
E2-C2	Creep -Air	68	704	483	1531.7
C-T1	Creep -Air	69	704	793	146
C-T7	Creep -Air	71	704	690	457.4
C-T11	Creep -Air	71	704	896	33.9
50C-T2	Creep -Air	67	704	793	128.3
9C-T1	Creep -Air	68	704	793	117.8
9C-T7	Creep -Air	79	704	793	127
0A-T1	Creep -Air	68	704	690	349.9
0A-T7	Creep -Air	79	704	793	133.6
0F-T1	Creep -Air	68	704	896	28.3
0A-T3	Creep -Air	68	704	690	284.3
50C-TM1	Creep - Vacuum	77	704	896	90
50C-TM6	Creep - Vacuum	77	704	896	56.5
0F-T6	Creep - Vacuum	70	704	793	123
9C-T4	Creep - Vacuum	67	704	793	203
9D-T3	Creep - Vacuum	68	704	586	1255
0A-T4	Creep - Vacuum	67	704	690	271
E2-NC1	ComboCreep-Kt=2	68	704	793	141.7
E2-NC2	ComboCreep-Kt=2	66	704	793	132.15
E2-NC3	ComboCreep-Kt=2	68	704	793	127.2
E2-NC4	ComboCreep-Kt=2	71	704	793	110.3
E2-NC5	ComboCreep-Kt=2	67	704	793	123.6
E2-NC6	ComboCreep-Kt=2	71	704	793	128.2
C-R2	Notch Rupture Kt=2	72	704	690	1105
C-R3	Notch Rupture Kt=2	77	704	793	620
C-R4	Notch Rupture Kt=2	77	704	793	1590
C-R7	Notch Rupture Kt=2	69	704	896	313
50C-R1	Notch Rupture Kt=2	77	704	690	809
50C-R2	Notch Rupture Kt=2	78	704	793	506

TABLE III.—DISTANCE FROM THE NOTCH ROOT TO THE CRACK ORIGIN FOR CYCLIC MAX DWELL NLCF TESTS

Specimen	Life, hr	Distance from notch, mm
E2-N1	955	2.4
E2-N2	978	2.6
E2-N3	625	1.6
E2-N6	610	1.5
E2-CN11	820	2.4
E2-CN13	780	2.6
9D-L5 Vac	1180	1

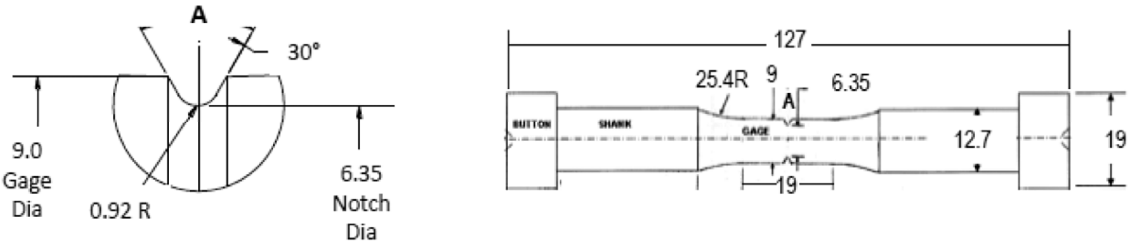

Figure 1.—Notched LCF specimen.

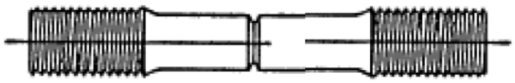

Figure 2.—Stress rupture specimen geometry.

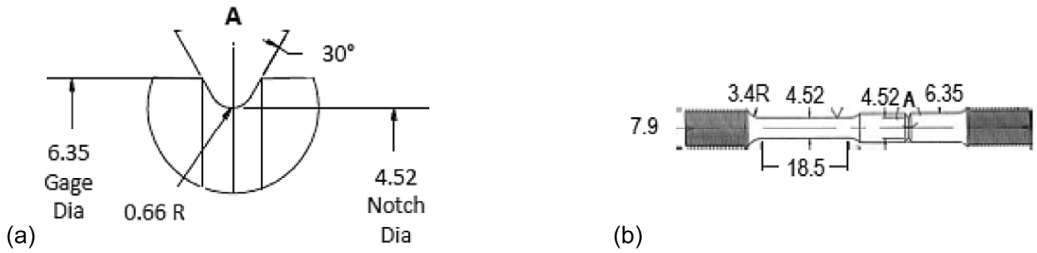

Figure 3.—Combo-bar specimen geometry. (a) Notch detail; (b) Specimen geometry.

Figure 4.—The two dwell cycles utilized for the NLCF testing. (a) Max dwell: 1.5-90-1.5s. (b) Min dwell: 1.5-1.5-90s.

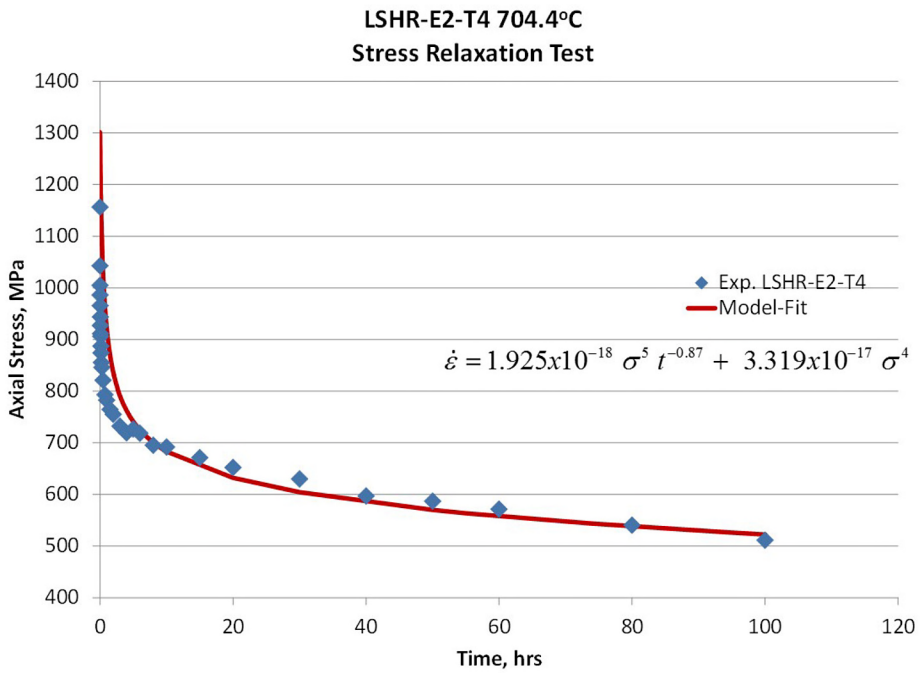

Figure 5.—Stress relaxation experiment and model fit.

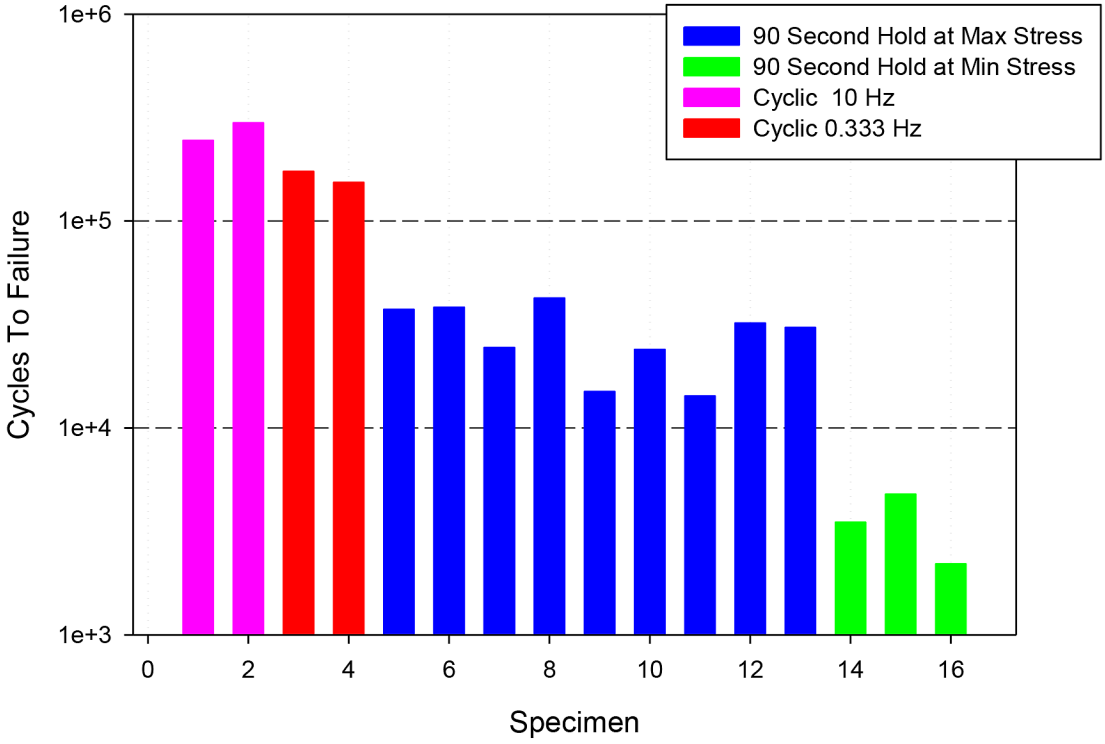

Figure 6.—Notched LCF results for cyclic and dwell tests performed in air at a maximum stress of 793 MPa.

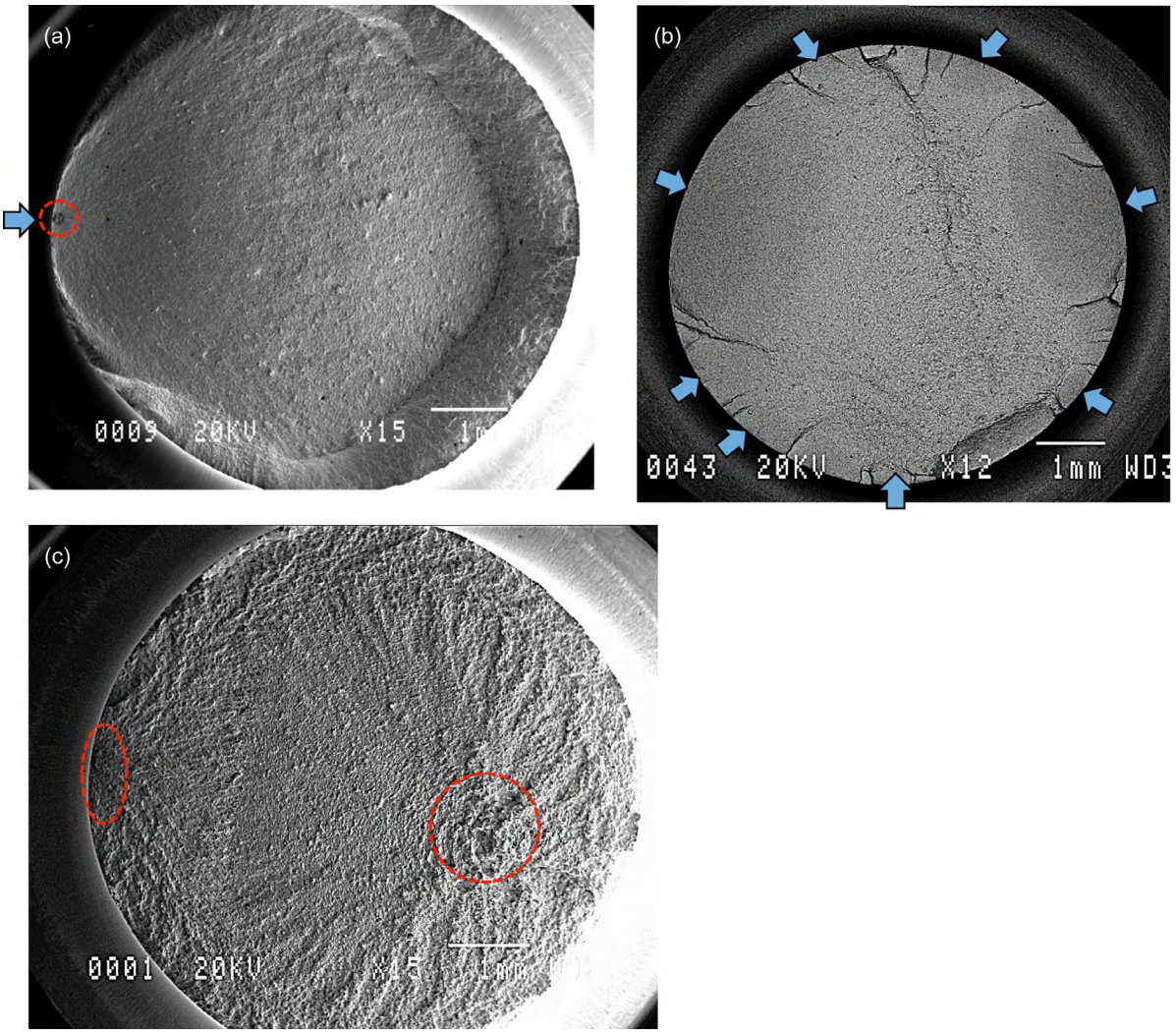

Figure 7.—Failure modes were drastically different for the cyclic and dwell NLCF tests performed at a max stress of 793 MPa. (a) Cyclic NLCF: 10 Hz. (b) Min dwell NLCF. (c) Max dwell NLCF.

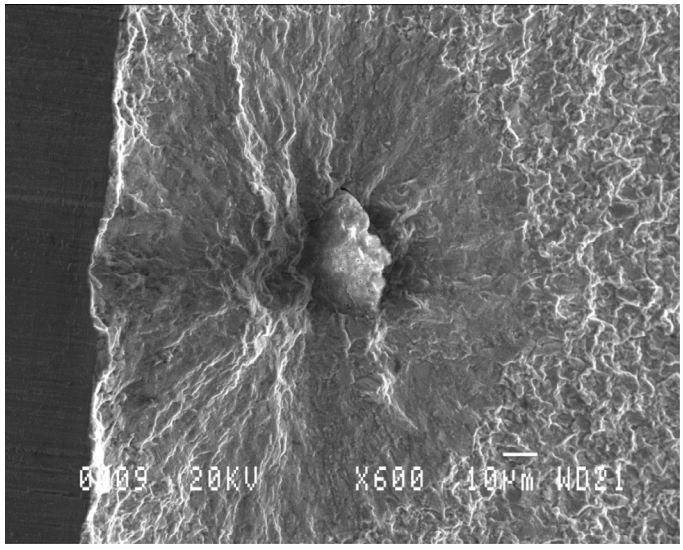

Figure 8.—Initiations in the cyclic NLCF tests originated at near surface ceramic inclusions.

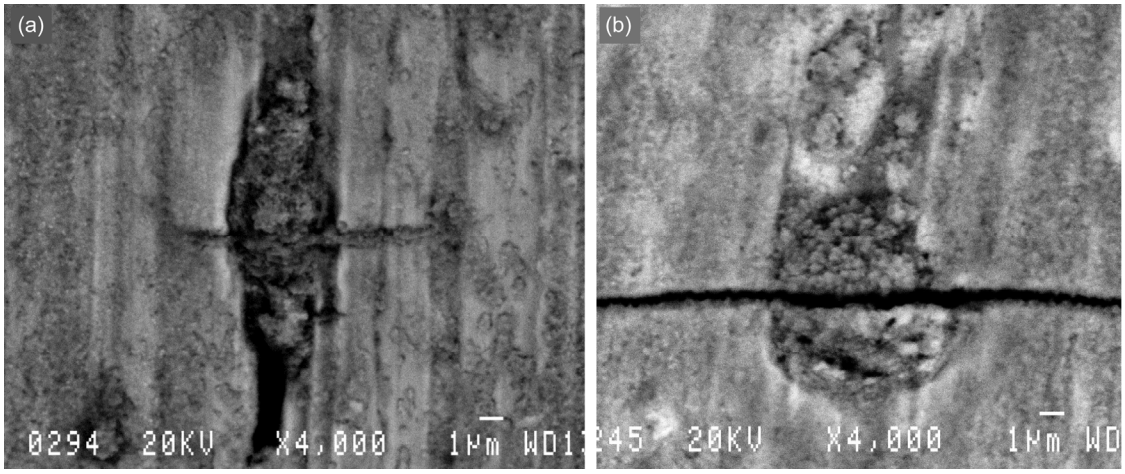

Figure 9.—Min dwell NLCF initiations occurred from microscopic oxide blisters.

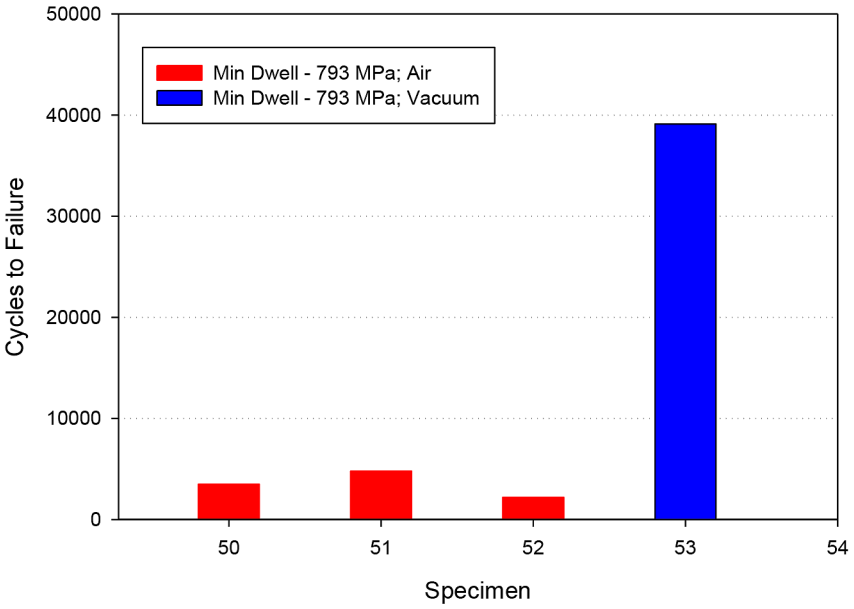

Figure 10.—Min dwell NLCF test results in air versus vacuum at a max stress of 793 MPa.

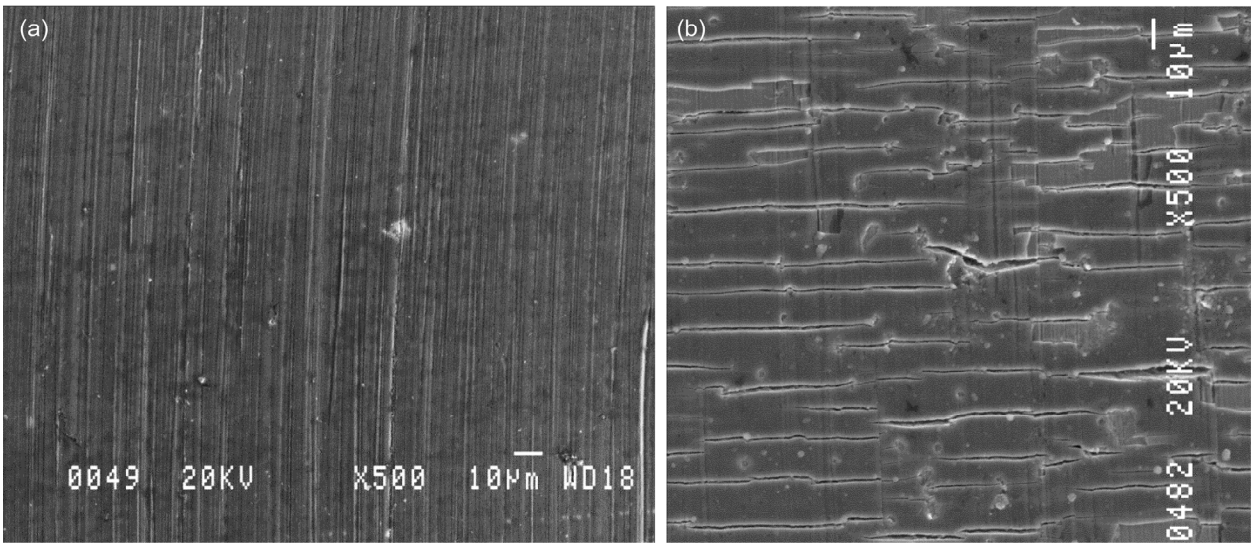

Figure 11.—Surface cracking in a vacuum notch min dwell test only occurred when an improper bake-out of a replacement heating element deposited a brittle coating on the surface of specimen. (a) Vacuum min dwell: 28,600 cycles. (b) Vacuum min dwell: 39,106 cycles.

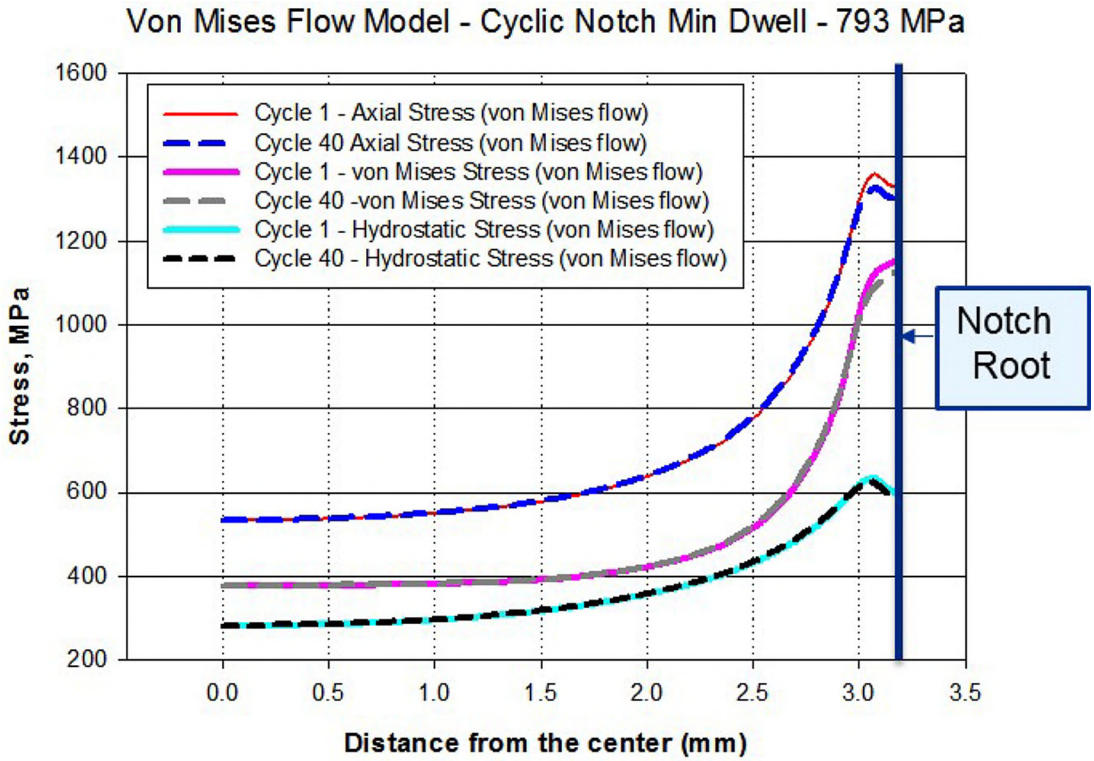

Figure 12.—Axial, von Mises and hydrostatic stress profiles remain almost unchanged after the first 40 min dwell NLCF cycles.

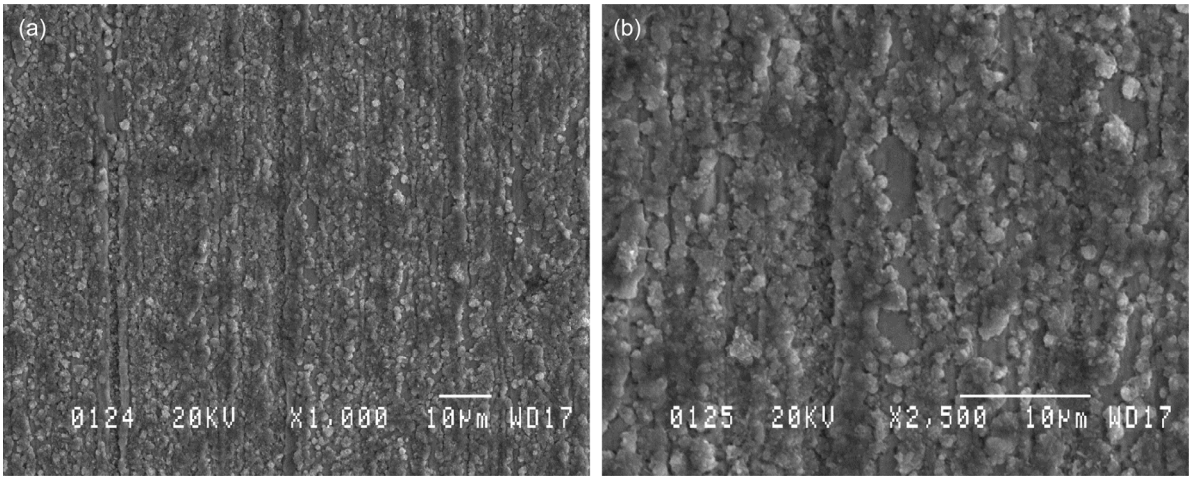

Figure 13.—Uniform gage specimen tested for 50,000 min dwell cycles at a max stress 793 MPa. Surface covered with oxide particles yet no surface cracking was detected. (a) Lower magnification. (b) Higher magnification.

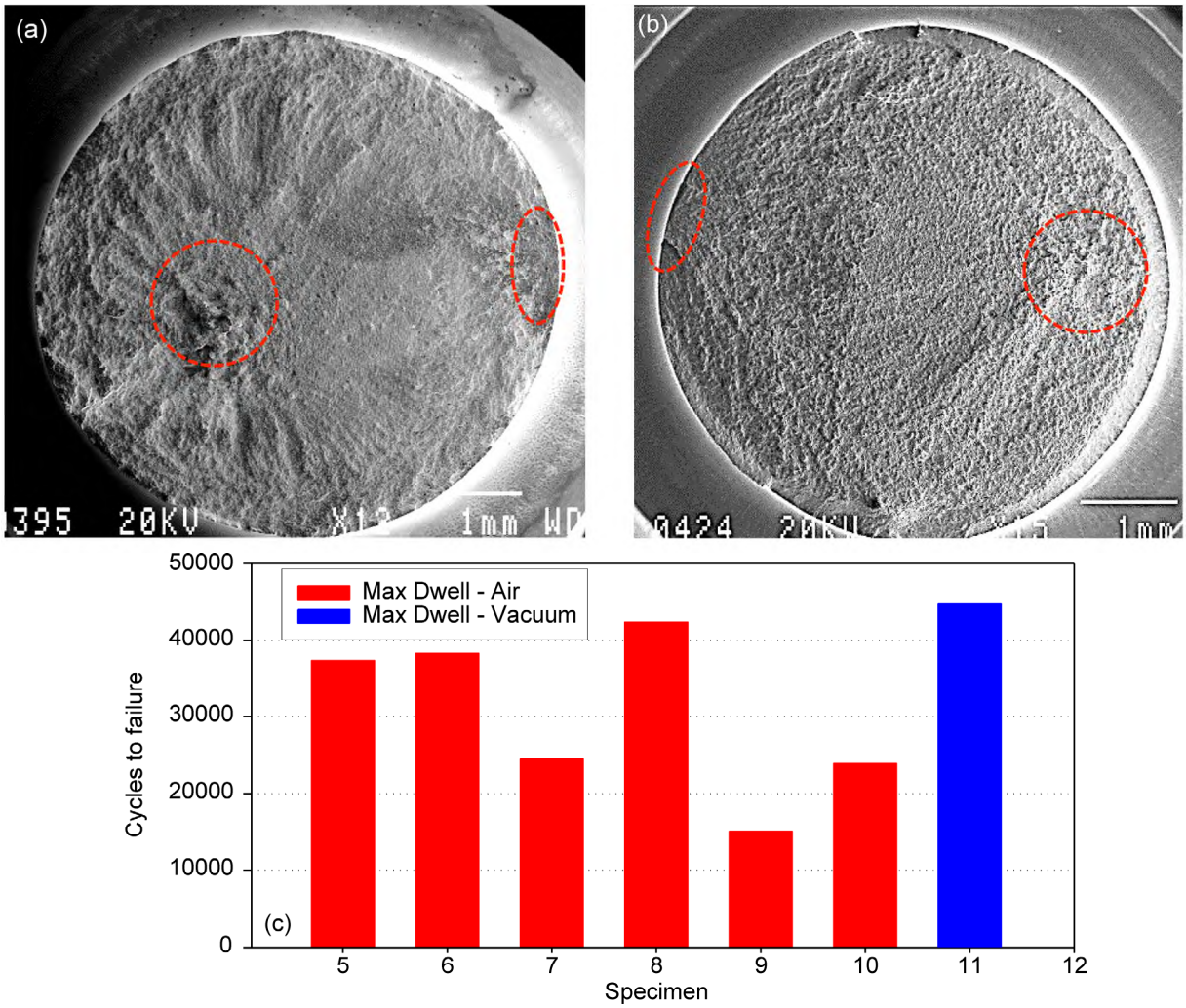

Figure 14.—Comparison of failure modes and dwell fatigue lives for air and vacuum tested cyclic max dwell NLCF specimens tested at 793 MPa. (a) Cyclic max dwell NLCF in air. (b) Cyclic max dwell NLCF in a vacuum. (c) Cyclic max dwell air versus vacuum.

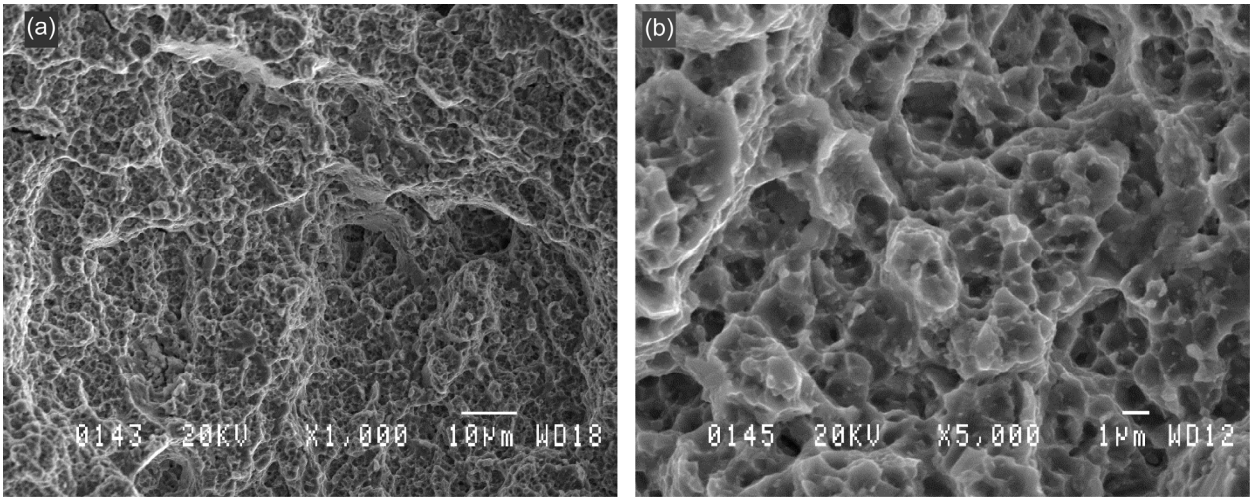

Figure 15.—Creep process deformation mechanisms observed at the internal initiation sites. (a) Lower magnification. (b) Higher magnification.

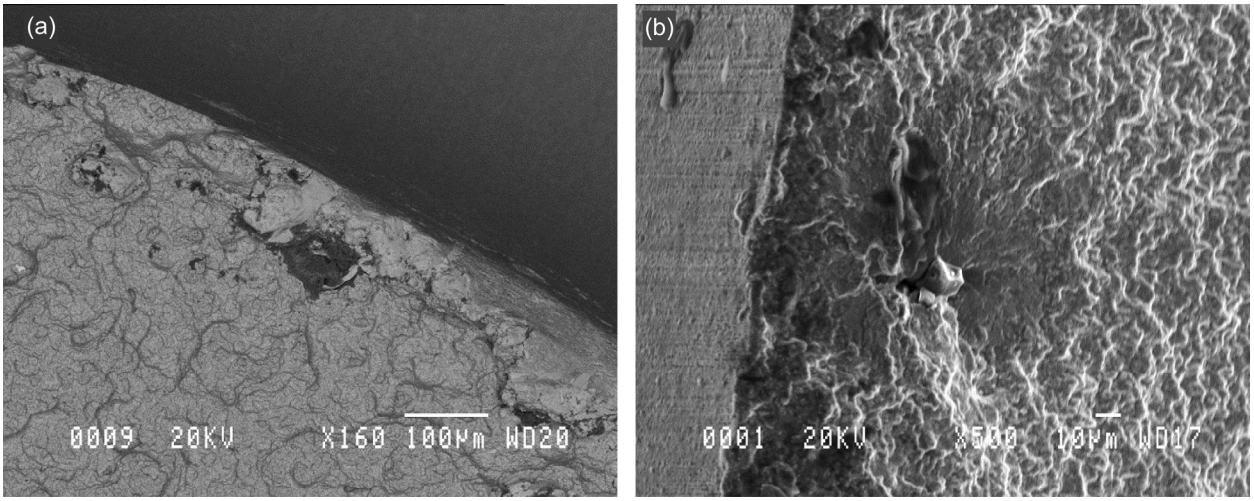

Figure 16.—Secondary initiations in the cyclic max dwell NLCF specimens typically occurred from near surface inclusions and are thought to be caused by a fatigue process. (a) Secondary initiation-near surface inclusion. (b) Near surface fatigue initiation.

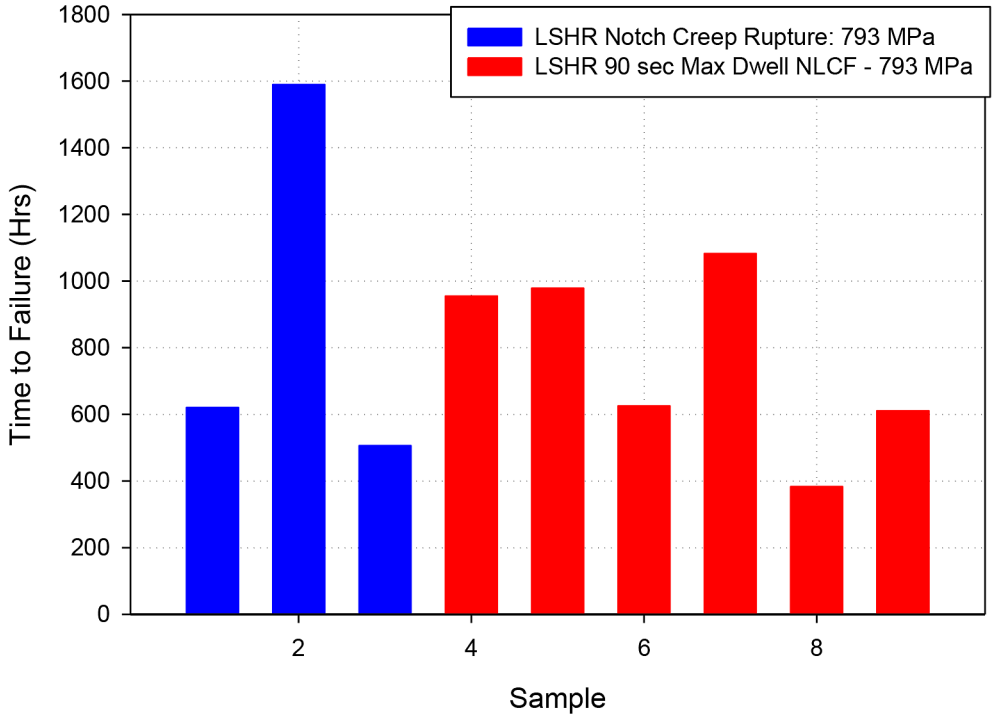

Figure 17.—Notch creep rupture lives were similar to the cyclic max dwell NLCF lives in terms of hours to rupture.

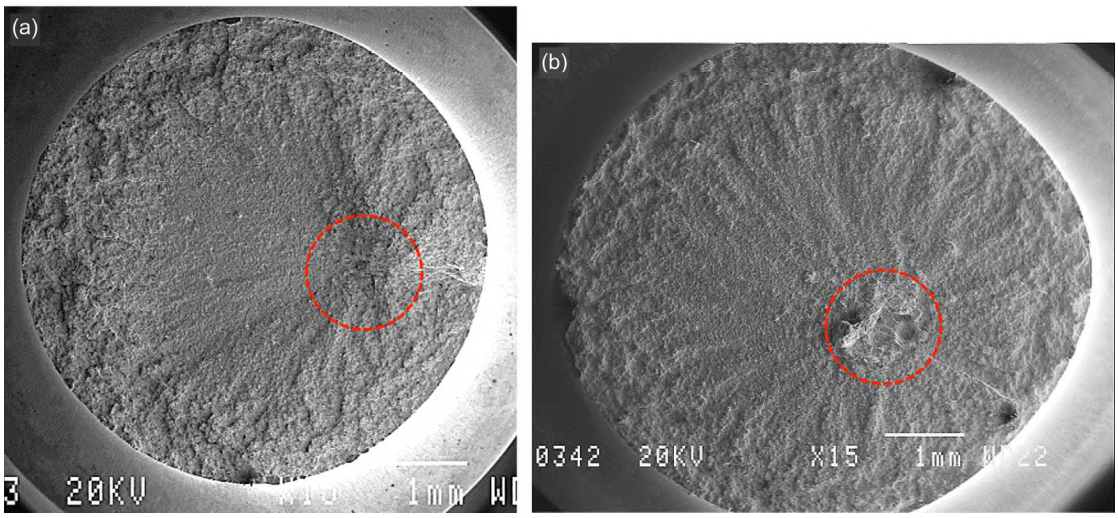

Figure 18.—Failure of notch rupture specimens tested at 793 MPa resulted from internal initiations similar to cyclic max dwell NLCF specimens. (a) Specimen A. (b) Specimen B.

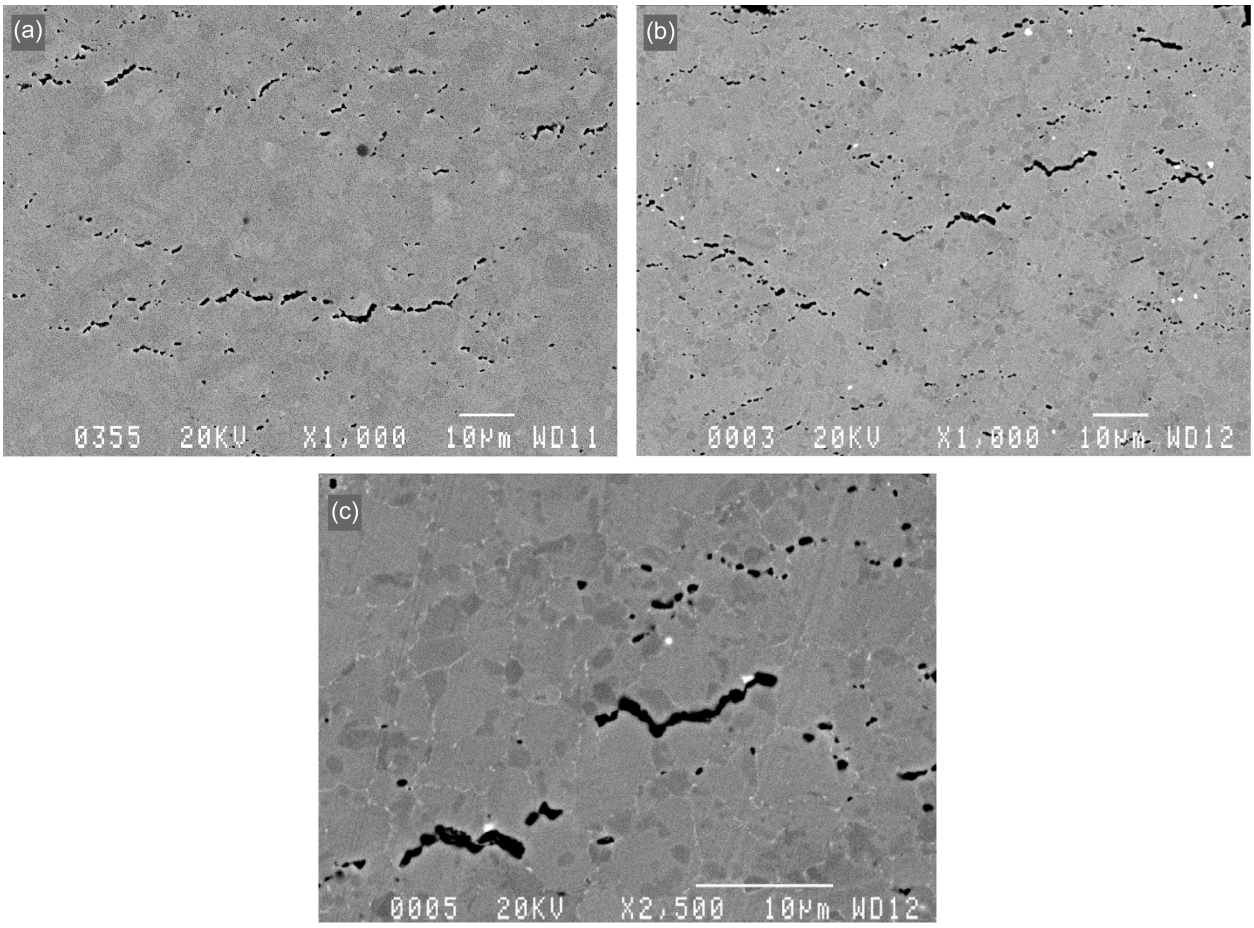

Figure 19.—Metallographic cross sections of notch rupture and cyclic max dwell NLCF specimens tested at 793 MPa, obtained from regions slightly below the internal crack initiation locations. Both types of specimens show creep rupture through grain boundary void coalescence. (a) Notch rupture. (b) Cyclic max dwell NLCF. (c) Cyclic max dwell NLCF at a higher magnification.

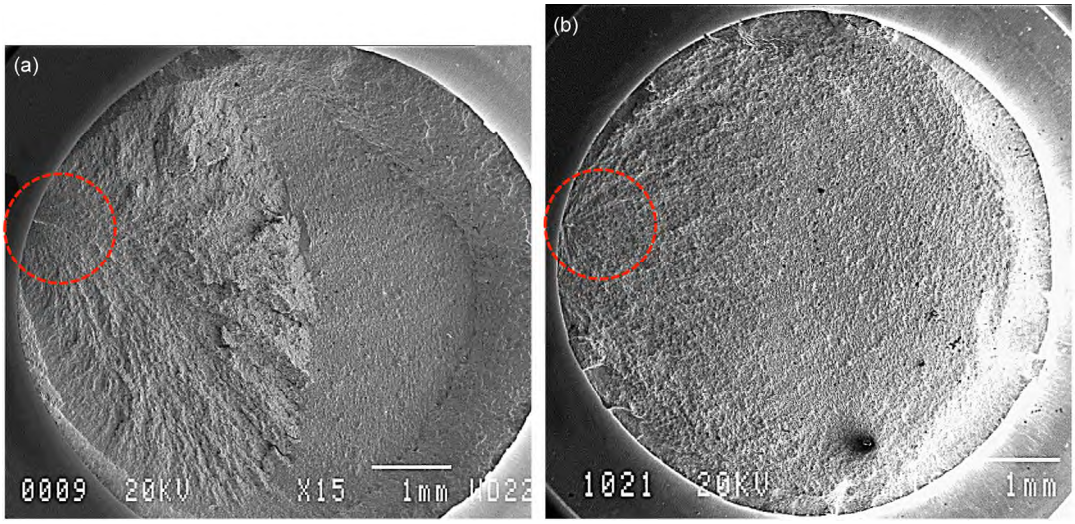

Figure 20.—Crack initiation for cyclic max dwell NLCF tested at 896 MPa occurred near the notch root both in air and vacuum. (a) Cyclic max dwell NLCF in air. (b) Cyclic max dwell NLCF in a vacuum.

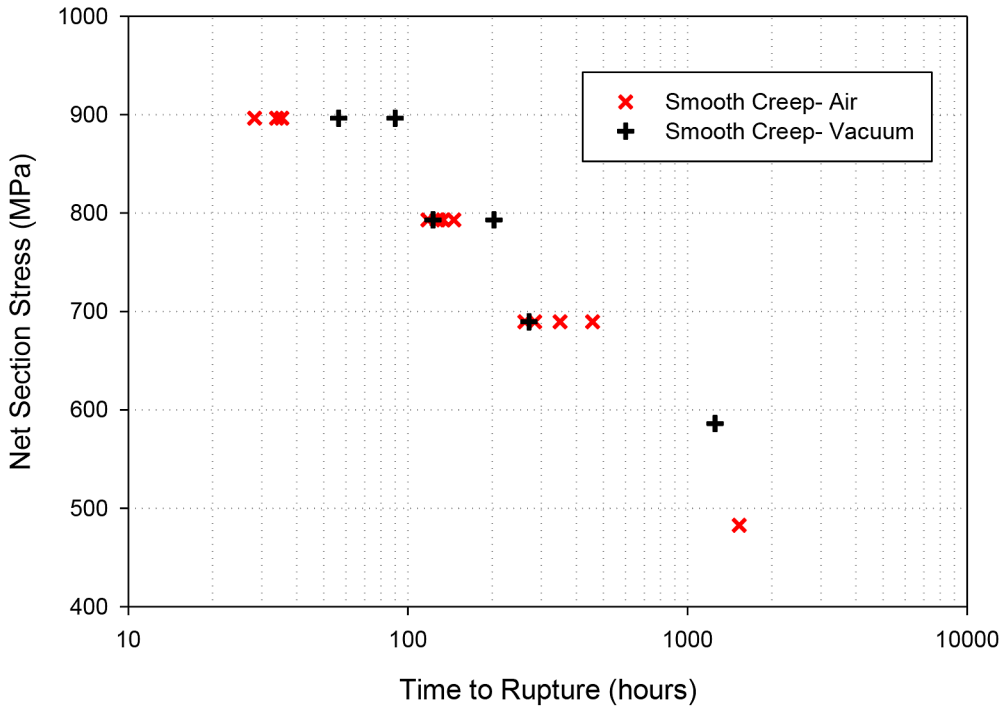

Figure 21.—Comparison of uniform gage creep behavior in air versus vacuum at 704 °C.

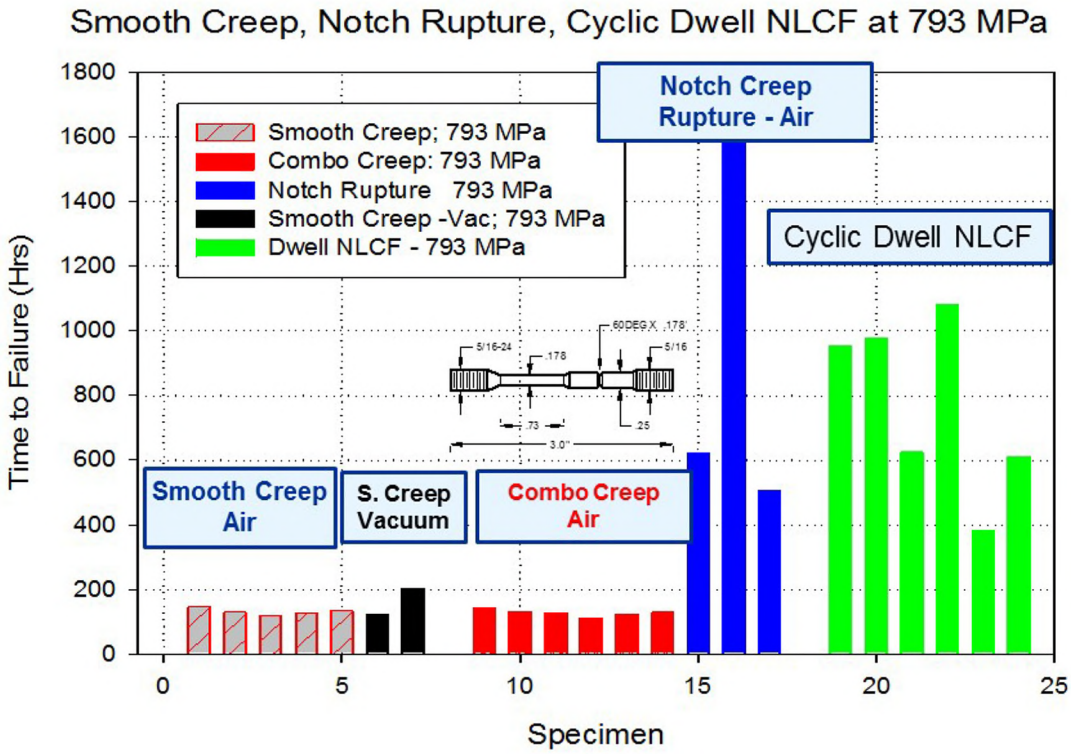

Figure 22.—Comparison of combo-bar rupture lives versus smooth creep and notched specimens. All combo-bar specimens failed in the smooth section.

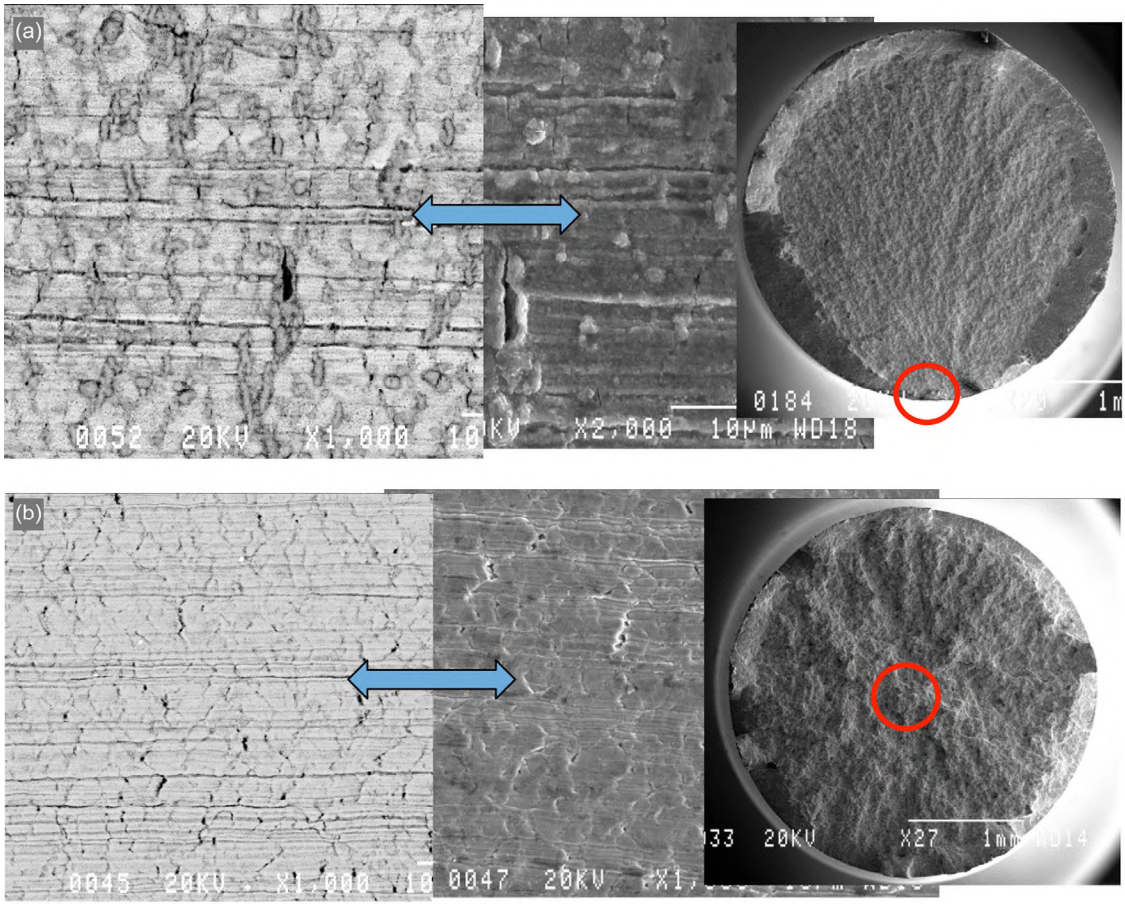

Figure 23.—Differences in surface deformation mode between uniform gage creep tests. (a) In air. (b) In a vacuum.

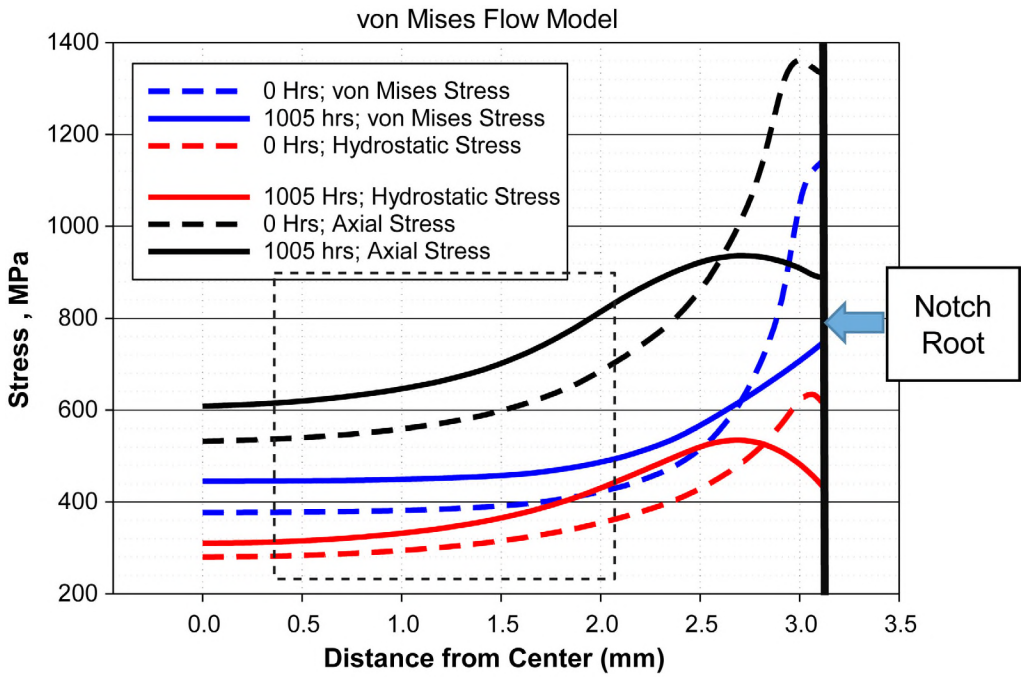

Figure 24.—Distribution profile of axial, von Mises and hydrostatic stresses based on von Mises plasticity flow model at 0 and 1000 hr of applied dwell at 793 MPa. Dotted box represents the distribution of the observed crack initiation sites in cyclic max dwell NLCF tests.

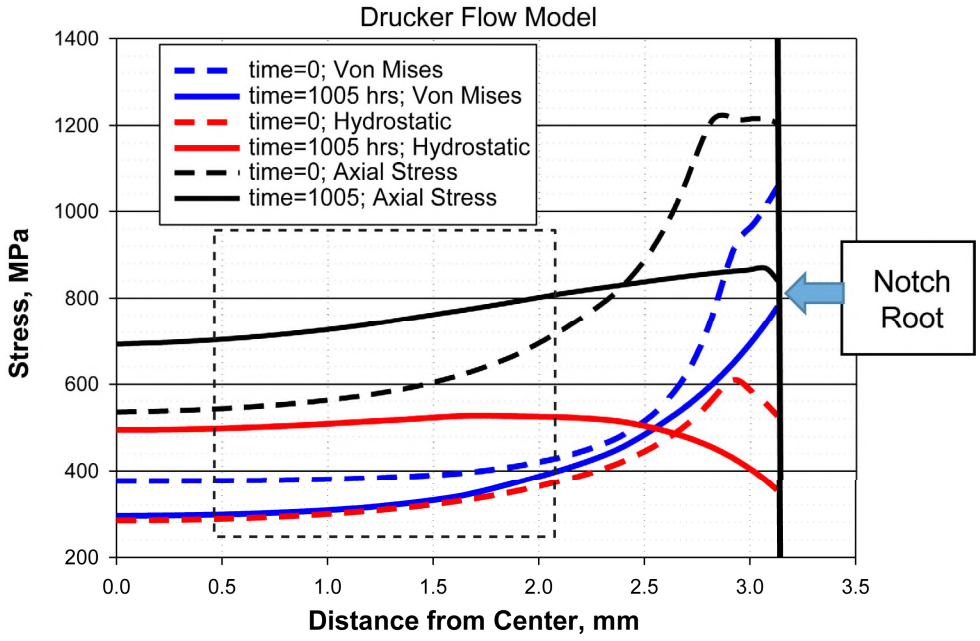

Figure 25.—Distribution profile of axial, von Mises and hydrostatic stresses based on Drucker-Prager plastic flow model at 0 and 1000 hr of dwell at 793 MPa. Dotted box represents the distribution of the observed crack initiation sites in cyclic max dwell NLCF tests.

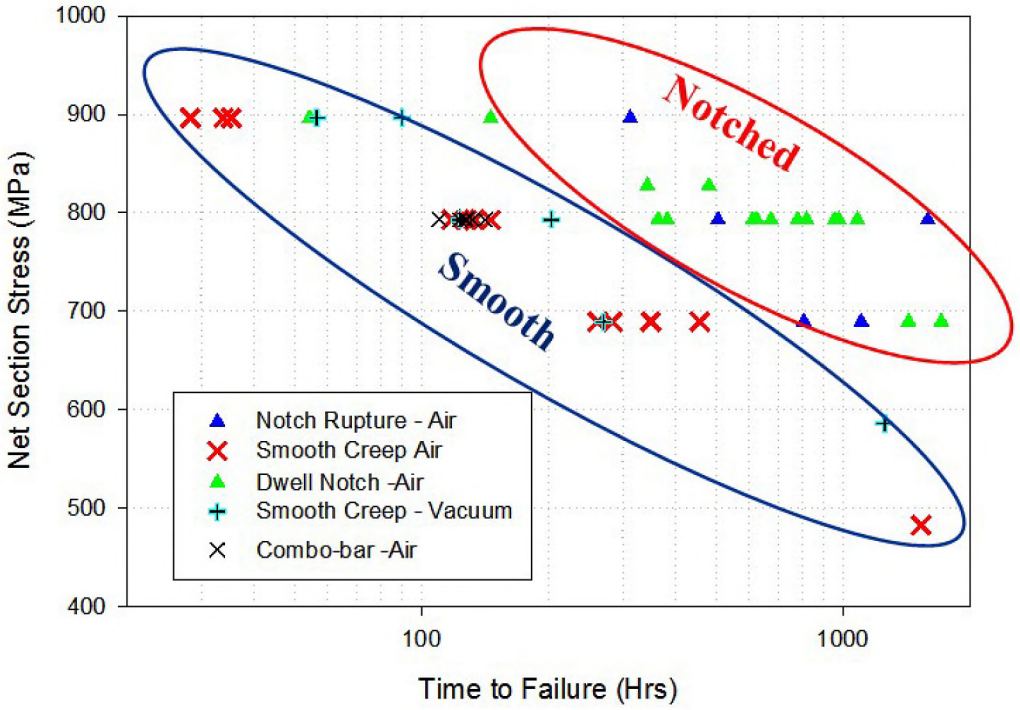

Figure 26.—Notch cyclic max dwell and creep notch rupture test exhibited longer life than uniform gage creep and combo-bar tests in terms of net section stress. Notch creep strengthening observed.

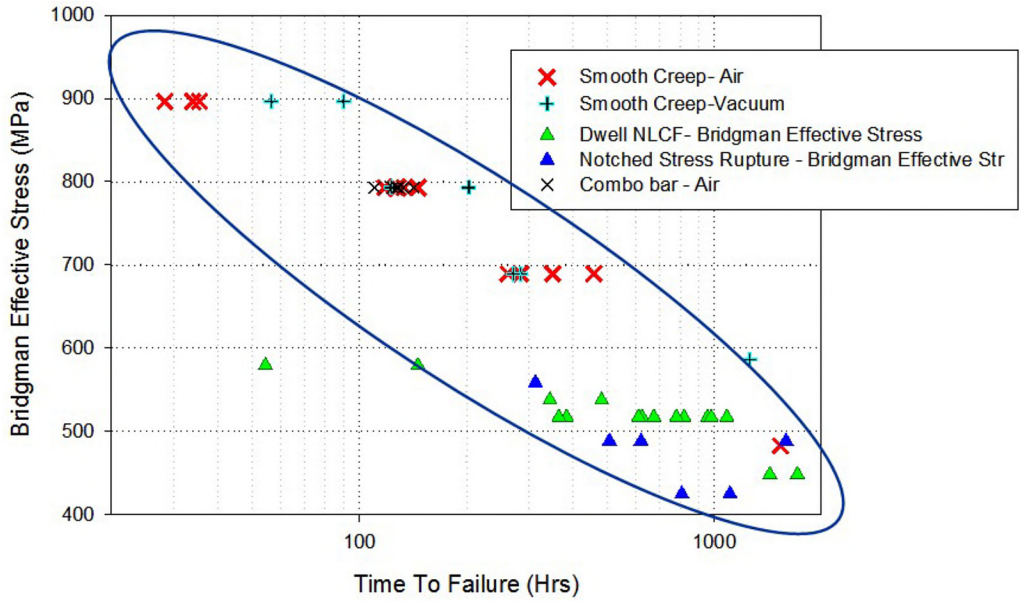

Figure 27.—Notch and uniform gage test data plotted in terms of the Bridgman effective stress. Methodology adequately accounts for visco-plastic notch strengthening.